European Radiology (2020) 30:3004–3014
https://doi.org/10.1007/s00330-019-06585-y

IMAGING INFORMATICS AND ARTIFICIAL INTELLIGENCE

A radiomics-based biomarker for cytokeratin 19 status of hepatocellular carcinoma with gadoxetic acid–enhanced MRI

Wentao Wang[1] · Dongsheng Gu[2,3] · Jingwei Wei[2,3] · Ying Ding[1] · Li Yang[1] · Kai Zhu[4] · Rongkui Luo[5] · Sheng-Xiang Rao[1] · Jie Tian[2,3,6,7] · Mengsu Zeng[1]

Received: 7 June 2019 / Revised: 14 October 2019 / Accepted: 11 November 2019 / Published online: 30 January 2020

Abstract

Objectives We aimed to develop a radiomics-based model derived from gadoxetic acid–enhanced MR images to preoperatively identify cytokeratin (CK) 19 status of hepatocellular carcinoma (HCC).

Methods A cohort of 227 patients with single HCC was classified into a training set (n = 159) and a time-independent validated set (n = 68). A total of 647 radiomic features were extracted from multi-sequence MR images. The least absolute shrinkage and selection operator regression and decision tree methods were utilized for feature selection and radiomics signature construction. A multivariable logistic regression model incorporating clinico-radiological features and the fusion radiomics signature was built for prediction of CK19 status by evaluating area under curve (AUC).

Results In the whole cohort, 57 patients were CK19 positive and 170 patients were CK19 negative. By combining 11 and 6 radiomic features extracted in arterial phase and hepatobiliary phase images, respectively, a fusion radiomics signature achieved AUCs of 0.951 and 0.822 in training and validation datasets. The final combined model integrated a-fetoprotein levels, arterial rim enhancement pattern, irregular tumor margin, and the fusion radiomics signature, with a sensitivity of 0.818 and specificity of 0.974 in the training cohort and that of 0.769 and 0.818 in the validated cohort. The nomogram based on the combined model showed satisfactory prediction performance in training (C-index 0.959) and validation (C-index 0.846) dataset.

Conclusions The combined model based on a fusion radiomics signature derived from arterial and hepatobiliary phase images of gadoxetic acid–enhanced MRI can be a reliable biomarker for CK19 status of HCC.

Key Points

- *Arterial rim enhancement pattern and irregular tumor margin on hepatobiliary phase on gadoxetic acid–enhanced MRI can be useful for evaluating CK19 status of HCC.*
- *A radiomics-based model performed better than the clinico-radiological model both in training and validation datasets for predicting CK19 status of HCC.*
- *The nomogram based on the fusion radiomics signature can be easily used for CK19 stratification of HCC.*

Wen-Tao Wang and Dong Sheng Gu contributed equally to this work

Electronic supplementary material The online version of this article (https://doi.org/10.1007/s00330-019-06585-y) contains supplementary material, which is available to authorized users.

✉ Jie Tian
tian@ieee.org

✉ Mengsu Zeng
zengmengsu@outlook.com

[1] Department of Radiology, Zhongshan Hospital, and Shanghai Medical Imaging Institute, Fudan University, 180 Fenglin Rd, Shanghai 200032, China

[2] Key Laboratory of Molecular Imaging, Institute of Automation, Chinese Academy of Sciences, 95 Zhongguancun East Road, Beijing 100190, China

[3] University of Chinese Academy of Sciences, Beijing 100049, China

[4] Liver Cancer Institute, Zhongshan Hospital, Fudan University, Shanghai, China

[5] Department of Pathology, Zhongshan Hospital, Fudan University, Shanghai, China

[6] Beijing Advanced Innovation Center for Big Data-Based Precision Medicine, School of Medicine, Beihang University, Beijing 100191, China

[7] Engineering Research Center of Molecular and Neuro Imaging of Ministry of Education, School of Life Science and Technology, Xidian University, Xi'an 710126, Shaanxi, China

Keywords Diagnosis · Cytokeratin 19 · Hepatocellular carcinoma

Abbreviations

ADC	Apparent diffusion coefficient
AUC	Area under curve
CK	Cytokeratin
DWI	Diffusion-weighted imaging
FOV	Field of view
HBP	Hepatobiliary phase
HCC	Hepatocellular carcinoma
HPC	Hepatic progenitor cell
ICC	Inter-correlation coefficient
LASSO	Least absolute shrinkage and selection operator
MRI	Magnetic resonance imaging
MS	Milliseconds
NRI	Net reclassification improvement
PVP	Portal venous phase
TE	Echo time
TR	Repetition time

Introduction

Hepatocellular carcinoma (HCC) is the most common liver cancer with a high incidence of cancer-related death worldwide [1–3]. Barcelona Clinic Liver Cancer (BCLC) staging system is recommended for outcome estimation and treatment proposals [4]. In practice, HCC patients within the same clinical classification have a distinct variable outcome even after curative treatment. Molecular profiling is expected to be incorporated in the staging system because HCC is a heterogeneous entity of various molecular phenotypes with an origin of hepatocytes and/or hepatic progenitor cells [5]. Molecular classification can help understand the biological behavior of tumor and optimize therapy [4–6].

Cytokeratins (CKs) are intermediate filament proteins expressed in epithelial cells [7]. In adult liver, hepatocytes express CK8 and CK18, whereas cholangiocytes additionally present CK7 and CK19 [8, 9]. There is growing evidence that HCC expressing biliary-specific markers (CK7 and CK19) is a subtype of hepatic progenitor cell (HPCs) origin. Especially, CK19-positive HCC was associated with clinical aggressiveness due to more tumor invasion [10], higher rate of lymph node metastasis [11, 12], and poorer prognosis after resection and liver transplantation [9, 13, 14]. This molecular subtype was suggested as a novel separate entity of HCCs and should be differentiated from other intermediate tumors showing HPC features such as cholangiolocellular carcinoma and combined HCC-cholangiocarcinoma [5, 10]. Therefore, identification of CK19 status of HCC holds promises for a better understanding of tumor biology and outcome estimation [15, 16].

Radiogenomics is a promising field for relating imaging traits to molecular portraits of HCC, by decoding gene expression [17, 18]. With a hypothesis of inferring gene-protein signatures from imaging features, radiomics is linked with the concept of radiogenomics [19]. Radiomics can comprehensively incorporate multiple biomarkers and facilitate a valuable predictive and validated model to guide clinical decision-making for HCC [20, 21]. Recently, several studies [22, 23] reported that CK19-positive HCC has characteristic imaging features on gadoxetic acid–enhanced magnetic resonance imaging (MRI) and one of them [22] reported a predictive model combining four criteria with very high specificity but unacceptable sensitivity. In addition, a proposed multiparametric MRI heterogeneity analysis of HCC showed significant correlations with gene expression level of CK19 [24]. To our knowledge, few study proposed a noninvasive and comprehensive model for CK19 status of HCC with satisfactory prediction performance.

In the present study, we aimed to preoperatively develop and validate a combined model integrating clinicopathological factors and radiomics signatures for better predicting CK19 status of HCC.

Material and methods

Patient population

The retrospective study was approved by our Institutional Review Board (approval number B2018-236) and the requirement for informed consent was waived. The study cohort was collected from our institutional radiology and pathology database between March 2012 and December 2017. A cohort of 589 consecutive patients with suspected HCCs underwent preoperative gadoxetic acid–enhanced MR imaging and subsequent hepatic resection. Only patients pathologically confirmed of having single primary HCC were included in our analysis. The exclusion criteria were as follows: patients receiving prior anticancer therapy such as chemoembolization, radiofrequency ablation, or transcatheter arterial chemoembolization (n = 169); with more than single HCC according to pathologic reports (n = 45); having cancerous thrombus in the portal vein, hepatic vein, or bile duct (n = 27), or having extrahepatic metastasis (n = 43); histologically diagnosed of high-grade dysplastic nodule (n = 9) or cholangiocarcinoma (n = 45); unrecorded pathologic findings of CK19 (n = 17); and time interval between MRI examination and surgery > 2 weeks (n = 7). Each patient was then categorized into the CK19-positive or CK19-negative expression group.

All enrolled patients received the curative resection. The tumor specimens were taken from the tumor and the surrounding liver tissues in a ratio of 1:1, at the 12, 3, 6, and 9 o'clock reference positions [25], with suitable formalin-fixed and paraffin-embedded. Pathological characteristics including tumor size and number, the presence of cirrhosis, microvascular invasion, and Edmondson-Steiner grade were assessed. The routine immunochemical staining for CK19 was assessed in consensus by two experienced pathologists in a team of pathologists, using a two-step protocol (Novolink Polymer Detection System) as previously described [26, 27]. A multihead microscope was used when the two pathologists had discrepancies. Monoclonal antibodies against human CK19 (DakoCytomation) were used at a dilution of 1:50. CK19-positive expression was defined as membranous or cytoplasmic immunoreactivity presented in ≥ 5% of tumor cells [8].

MRI data

The gadoxetic acid–enhanced MR images were obtained in a 1.5-T scanner (Magnetom Aera; Siemens Healthineers). Baseline sequences included diffusion-weighted imaging (DWI), T2-weighted phase, pre-contrast T1-weighted phase, dynamic T1-weighted arterial phase, portal venous phase, delayed phase, and hepatobiliary phase (HBP). A prototype single-shot spin echo echo-planar free-breathing DWI sequence using repetition time (TR), 5100 milliseconds (ms); echo time (TE), 55 ms; field of view (FOV), 285 × 380 mm; matrix size, 192 × 154; and slice thickness, 5.5 mm was acquired before the dynamic examination. A corresponding apparent diffusion coefficient (ADC) map was automatically calculated with two *b* values of 0 and 500 s/mm^2. For dynamic T1-weighted examination, we used the parameters TR, 3.47 ms; TE, 1.36 ms; flip angle, 10°; FOV, 308 × 380 mm; matrix size, 320 × 240; and slice thickness, 3 mm. After an intravenous injection of 0.025 mmol/kg of gadoxetic acid (Primovist, Bayer) at a speed of 2 mL/s, we obtained images of arterial phase, portal venous phase (PVP), delayed phase, and HBP in 20–30 s, 60–70 s, 180 s, and 20 min, respectively. T2-weighted images (TR, 4918 ms; TE, 106 ms; FOV, 285 × 380 mm; matrix size, 384 × 273; slice thickness, 5.5 mm) were obtained during the interval between delayed phase and hepatobiliary phase.

Morphologic features of MR images

The morphologic features were evaluated on a picture archiving and communication system (Centricity RA1000, General Electric) by two dedicated radiologists (S.X.R. and Y.D., with 20 and 15 years of experience, respectively) in consensus and they were both blinded to the histopathologic results. Any disagreement would be discussed until a final consensus was generated. The interobserver agreements of morphologic MR features were provided in Supplemental Table 1. Qualitative imaging parameters of each HCC were evaluated as follows: (a) presence of smooth or irregular tumor margin. Irregular tumor margin was defined as extranodular budding portion on transverse HBP images; (b) dynamic enhancement pattern, categorized as arterial enhancement with washout (visually arterial phase hyperenhancement combined with subsequent hypointensity on PVP), persistent enhancement, progressive enhancement, and no or minimal enhancement; (c) arterial rim enhancement, defined as central hypointense areas with peripheric ring-like enhancement on arterial phase; (d) presence of radiological capsule; (e) fat deposition.

MR image segmentation

The whole tumor segmentation was performed in ITK-SNAP software (http://www.radiantviewer.com) by a radiologist with 8 years of experience, and then validated by an experienced radiologist with 25 years of experience. Regions of interests (ROIs) were manually outlined along the edge of tumor on the T2-weighted images, *b* values of 500 s/mm^2 DW images, ADC maps, pre-contrast T1-weighted phase, dynamic arterial phase, portal venous phase, delayed phase, and hepatobiliary phase images, respectively. To test the reproducibility of signature mining by a test-retest procedure, we randomly selected a cohort of 20 HCCs to perform repeat segmentation.

Clinical and morphologic risk features

Univariable analysis was used to assess the association between clinical, morphologic features and CK19 status of HCC. The backward stepwise selection using the stopping rule Akaike's information criterion with all variables was performed by multivariable logistic regression analysis. Variables with a p value < 0.05 in the multivariate analysis were identified as potential clinical and morphologic risk factors and the clinical model based on these factors was constructed at the same time.

Radiomic feature analysis

The procedure of radiomic feature analysis includes feature extraction and feature selection.

Firstly, MR images of all the eight sequences were imported into the open-source software platform "Pyradiomics 1.3.0" (http://www.radiomics.io/pyradiomics.html), which can extract quantitative features with a series of feature extraction algorithms for medical images [28]. A total of 647 features were extracted for further analysis.

Secondly, the reproducibility of all the radiomic features in intra- and inter-observer was assessed by intra- and inter-

correlation coefficient (ICC) [29]. Features with ICC greater than 0.8 were considered reproducible and included in the following feature selection. Next, the least absolute shrinkage and selection operator (LASSO) regression model was utilized for feature selection. This method is a regularization for multivariable logistic model, which can obtain the best feature set with optimal cross-validation performance [30].

Model building

Decision tree was adopted for further radiomics signature building with the radiomic features that chosen by LASSO. By constructing a decision tree with a series of branches and leaves, the decision tree learning algorithm could go from observations to the predicted target value [31]. Leave-one-out cross-validation was employed for the best parameter selection in our training dataset; parameters with the optimal mean area under curve (AUC) was chosen for the radiomics signature building. For every single phase, the mean AUC of leave-one-out cross-validation in training cohort was obtained, and those phases with AUC greater than 0.700 were considered significant and thus included for the fusion radiomics signature building.

To test whether the radiomics signature and clinical factors were complementary for the prediction of CK19 status, we created a combined model integrating all the potential factors together to a multivariable logistic regression model. Clinical factors with significant association with CK19 were entered into the multivariable combined model along with radiomics signature. AUCs were used to quantify the discriminative ability for classifier model and the performances of the three models were compared using the Delong test. Hosmer-Lemeshow test was performed to identify the agreement between predicted probability of the combined model and the observed status of CK19. Net reclassification improvement (NRI) analysis was used to assess the increased value of the radiomics signature and combined model compared with the clinical model separately. The nomogram based on the predictive combined model was established for the easy use to generate a probability of CK19 status.

Flowchart of tumor segmentation, feature extraction, and model building was shown in Fig. 1.

Statistical analysis

The statistical differences of variables were analyzed in the training and validation datasets using *t* test or Mann-Whitney *U* test for continuous variable and chi-square test for qualitative variable. The statistical analyses were conducted with the software of IBM SPSS Statistics 20 and R software (version 3.4.1). All the statistical tests were two-side. *P* values less than 0.05 were regarded as statistically significant.

Results

Clinicopathologic and morphologic features

Comparisons of demographic, laboratory, and morphological imaging features between training and validated patients were shown in Table 1. The final cohort of 227 patients (198 men and 29 women) with single HCC was classified into a training set (n = 159, 40 for CK19 positive, 119 for CK19 negative; 136 men and 23 women; March 2012–March 2017) and a time-independent validated set (n = 68, 17 for CK19 positive, 51 for CK19 negative; 62 men and 6 women; March 2017–December 2017). In the whole cohort, 57 (25.1%) patients were positive for CK19 and 170 (74.9%) patients were negative for CK19. There was no significant difference of the status of CK19 between training and validation dataset (p = 0.230). According to univariate analysis, CK19-positive HCCs were more likely to have higher serum α-fetoprotein (AFP) level (p < 0.001, OR 2.16, 95% CI 1.42–3.29), irregular margin (p = 0.004, OR 2.45, 95% CI 1.32–4.53), and arterial rim enhancement (p = 0.001, OR = 3.28, 95% CI = 1.59–6.74). At the multivariate analysis, serum AFP level (p = 0.001, OR 2.06, 95% CI 1.33–3.19), irregular tumor margin (p = 0.050, OR 1.93, 95% CI 1.00–3.70), and arterial rim enhancement (p = 0.011, OR 2.70, 95% CI 1.25–5.82) were all independent significant variables associated with CK19 expression (Table 2). The clinical model constructed with these factors had an AUC of 0.714 (95% CI 0.624–0.803) in the training dataset and 0.753 (95% CI 0.636–0.871) in the validation dataset.

Feature selection and radiomics model construction

After feature selection by reproducibility analysis, features derived from DWI and ADC maps were reduced to 0, meaning a pretty poor robustness. The further analysis of LASSO has eliminated all the robust features in T2-weighted and pre-contrast T1-weighted images. Accordingly, these 4 sequences of MR images were removed in our model construction. The feature numbers for each phase during the procedure of feature selection are shown in Table 3. Furthermore, all of the prediction performances for the four phases are presented in Table 4. In the end, as the cross-validation mean AUC for hepatobiliary phase, arterial phase, venous phase, and delay phase were, respectively, 0.893, 0.854, 0.512, and 0.478, we chose the radiomics signature of hepatobiliary phase and arterial phase (> 0.700) to be further analyzed. The distributions of radiomic features in both arterial phase and hepatobiliary phase images are shown in Supplementary Figure 1. Using the robust features, 11 and 6 features were considered the optimal feature set after LASSO modeling for the prediction of CK19 in the two phases, respectively. Next, a classifier model of decision tree was performed using the selected features. In arterial phase, the selected features included Coif1_glrlm_SRLGLE, Coif1_glrlm_energy,

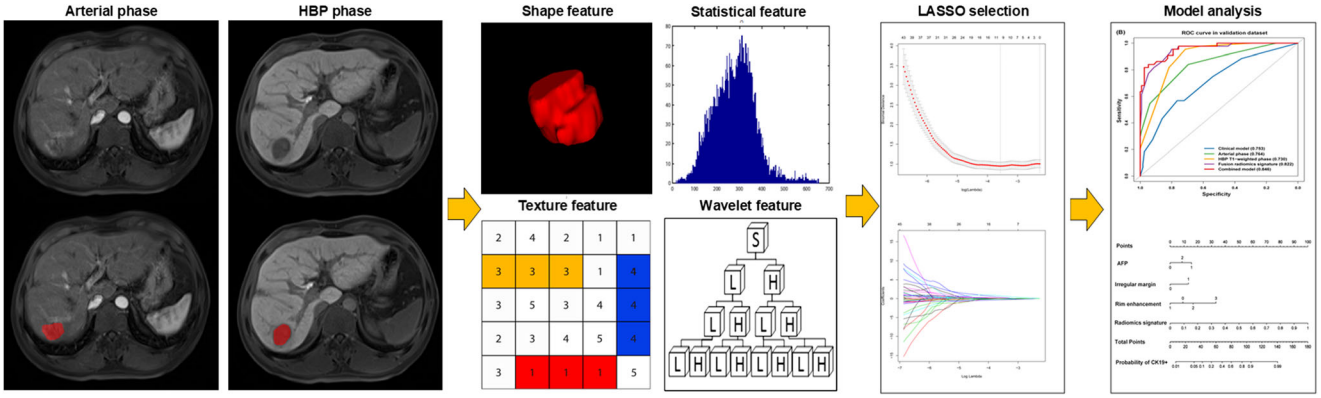

Fig. 1 Flowchart of tumor segmentation, feature extraction, and model building. Manual segmentation was performed in the multi-phase images, and the features can be divided into 4 groups, including shape, statistical, texture, and wavelet features. Next, least absolute shrinkage and selection operator (LASSO) was used for feature selection and model establishment. Receiver operating characteristic (ROC) curve and the nomogram for predicting CK19 status were then developed

Coif1_glszm_HGLZE, Coif1_glszm_LGLZE, Coif2_glszm_LZLGE, Coif3_glszm_ZSV, Coif5_glcm_variance, Coif5_glszm_ZSV, Coif7_glszm_ZSV, Coif8_glszm_ZSV, ori_fos_minimum. In hepatobiliary phase, the selected features comprised Coif1_glrlm_SRLGLE, Coif2_glszm_ZSNU, Coif4_glcm_cluster_tendency, Coif4_glszm_ZSV, Coif8_glszm_ZSNU, ori_Surface_to_volume_ratio. Detailed feature information is presented in Supplementary Table 2.

In the arterial phase, the radiomics signature yielded an AUC of 0.847 (95% CI 0.779–0.915) in the training dataset and 0.764 (95% CI 0.636–0.893) in the validation dataset. Similarly, the radiomics signature of hepatobiliary phase yielded an AUC of 0.892 (95% CI 0.847–0.937) and 0.730 (95% CI 0.578–0.882) in training and validation set separately. In addition, to make the full potential value of both the radiomics signature in different sequences, we built a fusion radiomics signature, which integrates the radiomics signatures in the two phases with the multivariable logistic regression model. The fusion radiomics signature expectedly achieved a satisfying performance with an AUC of 0.951 (95% CI 0.917–0.985) and 0.822 (95% CI 0.716–0.928) in training and validation datasets. The Delong test manifested significant difference when the fusion radiomics signature was compared with clinical model in the training dataset ($p < 0.001$); however, in the validation dataset, the p value is 0.168. There were significant differences of the distribution of the fusion radiomics signatures between CK19-positive and CK19-negative groups in both training ($p < 0.001$) and validation ($p < 0.001$) datasets (Fig. 2).

Predictive model development

The final combined model integrating all the potential factors including significant clinical variables (serum AFP levels, arterial rim enhancement pattern, and irregular tumor margin) and the fusion radiomics signature obtained the best performance for CK19 prediction. The classification performance of the combined model performed better than clinical model alone in the training (0.959 [0.929–0.989] vs. 0.714 [0.624–0.803]; $p < 0.001$) and validation (0.846 [0.730–0.963] vs. 0.753 [0.636–0.871]; $p = 0.047$) datasets. The radiomics signature yield value increased compared with clinical model in the training (NRI, 1.432, $p < 0.001$) and validation dataset (NRI, 0.965, $p < 0.001$). Additionally, integration of the radiomics signature into the prediction model showed significant improvement of predictive performance than clinical model in the training (NRI, 1.588, $p < 0.001$) and validation dataset (NRI, 1.038, $p < 0.001$). Comparisons between the combined model and each radiomics model of different phase are shown in Supplementary Table 3. Good agreement in both training ($p = 0.65$) and validation ($p = 0.22$) dataset were obtained. ROC curves of all the models for predicting CK19 are presented in Fig. 3, and the performances for each model are shown in Table 4. The nomogram (Fig. 4) showed satisfactory prediction performance in training (C-index 0.959 [95% CI 0.928–0.989]) and validation (C-index 0.846 [95% CI 0.733–0.959]) dataset.

Discussion

Our study established a predictive nomogram incorporating gadoxetic acid–enhanced MRI-based radiomics signatures, serum AFP level, irregular tumor margin, and arterial rim enhancement pattern for preoperatively identifying CK19-positive HCCs. The combined model demonstrated a satisfactory diagnostic performance for stratifying HCCs by CK19 status.

For identifying CK19-positive HCCs, the fusion radiomics signature achieved an AUCs of 0.951 in training cohort and 0.822 in validation cohort, better than the performance of radiomics signatures that separately extracted in arterial phase

Table 1 Comparison of CK19 status and characteristics in both training and validated HCC patients

Characteristics	No.	Training set (n = 159)		p value	No.	Test set (n = 68)		p value	p value*
		CK19 (+) (n = 40)	CK19 (−) (n = 119)			CK19 (+) (n = 17)	CK19 (−) (n = 51)		
Median age, years (range)	159	51 (24–75)	53 (27–75)	0.057	68	53 (34–83)	54 (26–74)	0.986	0.863
Gender				0.604				1.000	0.243
Male	136	33	103		62	15	47		
Female	23	7	16		6	2	4		
Tumor size, cm, mean and SD (range)	159	2.0 ± 1.0 (0.8–5.1)	2.3 ± 1.5 (0.9–8.4)	0.218	68	2.1 ± 1.1 (0.9–4.5)	1.8 ± 0.9 (0.7–5.5)	0.407	0.142
Etiology of liver disease				0.730				0.584	0.151
HBV positive[a]	143	36	107		65	16	49		
HCV positive[b]	7	1	6		1	0	1		
None or other	9	3	6		2	1	1		
Microvascular invasion				0.687				0.095	0.457
Presence	45	10	35		16	7	9		
Absence	114	30	84		52	10	42		
Edmondson-Steiner grade				0.436				0.262	0.141
I–II	108	25	83		34	6	28		
III–IV	51	15	36		34	11	23		
Satellite nodule				0.763				0.095	0.519
Presence	16	5	11		5	3	2		
Absence	143	35	108		63	14	49		
Growth type				0.013				0.213	0.080
Smooth margin	75	12	63		45	9	36		
Focal extranodular growth	54	19	35		19	6	13		
Multifocal nodular confluent	19	8	11		3	1	2		
Infiltrative growth	11	10	1		1	1	0		
Tumor capsule				0.261				1.000	0.977
Complete	126	29	97		54	14	40		
Incomplete or absent	33	11	22		14	3	11		
Background liver tissue				0.274				0.275	0.183
Liver cirrhosis	100	26	74		49	11	38		
Chronic hepatitis	50	10	40		16	4	12		
Normal	9	4	5		3	2	1		
Serum AFP				0.001				0.023	0.790
< 20 ng/mL	88	13	75		35	4	31		
20–400 ng/mL	51	17	34		25	10	15		
> 400 ng/mL	20	10	10		8	3	5		
Total bilirubin				1.000				0.669	0.393
≤ 20.4 μmol/L	146	37	109		60	16	44		
> 20.4 μmol/L	13	3	10		8	1	7		
Morphologic MR features									
Irregular margin on HBP				0.011				0.239	0.280
Absence	80	13	67		45	9	36		
Presence	79	27	52		23	8	15		
Enhancement pattern				0.007				0.130	0.582
Arterial enhancement with washout	127	28	99		56	11	45		
No or minimal enhancement	14	8	6		5	2	3		
Persistent enhancement	15	2	13		4	2	2		
Progressive enhancement	3	2	1		3	2	1		
Arterial rim enhancement				< 0.001				0.020	0.157
Presence	31	16	15		8	5	3		
Absence	128	24	104		60	12	48		
Fat deposition				0.310				1.000	0.051
Presence	42	8	34		8	2	6		
Absence	117	32	85		60	15	45		

[a] Represents positivity for hepatitis B serum antigen

[b] Represents positivity for serum HCV antibody

*Represents the comparisons of characteristics between training and validation cohorts.

No. represents number of training or validated patients

AFP, α-fetoprotein; *SD*, standard deviation; *HBP*, hepatobiliary phase

Table 2 Univariate and multivariate analyses of factors related with CK19 status

	No.	Univariate		Multivariate	
		p value	OR (95% CI)	*p* value	OR (95% CI)
Age	227	0.116	0.98 (0.95–1.01)		
Gender of male	198				
Tumor size	227	0.435	0.91 (0.71–1.16)		
Etiology of liver disease					
HBV positive	209	0.786	1.16 (0.39–3.41)		
Growth type					
Smooth nodular	120		1		
Focal extranodular growth	73	0.496	2.08 (0.25–17.13)		
Multifocal nodular confluent	22	0.116	5.44 (0.66–44.94)		
Infiltrative growth	12	0.071	7.69 (0.84–70.46)		
Microvascular invasion	61	0.562	1.22 (0.63–2.36)		
Edmondson-Steiner grade (III–IV)	85	0.361	1.30 (0.74–2.30)		
Presence of liver cirrhosis	149	0.894	0.96 (0.51–1.79)		
Serum AFP level	227	< 0.001	2.16 (1.42–3.29)	0.001	2.06 (1.33–3.19)
Total bilirubin > 20.4 μmol/L	21	0.503	0.68 (0.22–2.11)		
Irregular tumor margin	102	0.004	2.45 (1.32–4.53)	0.050	1.93 (1.00–3.70)
Enhancement pattern					
Arterial enhancement with washout	183	0.685	1.18 (0.54–2.56)		
No or minimal enhancement	19	0.335	0.54 (0.15–1.91)		
Persistent enhancement	19	0.899	1.07 (0.37–3.12)		
Progressive enhancement	6	0.640	1.51 (0.27–8.47)		
Tumor capsule	180	0.407	0.74 (0.36–1.51)		
Arterial rim enhancement	39	0.001	3.28 (1.59–6.74)	0.011	2.70 (1.25–5.82)
Fat deposition	50	0.347	0.69 (0.32–1.49)		

or hepatobiliary phase. In training cohort, the diagnostic accuracy of fusion radiomics signature reached 0.843; however, it decreased to 0.706 in validated cohort. After incorporating clinical and imaging biomarkers, the combined model achieved the highest diagnostic accuracy of 0.931 in training cohort and good accuracy of 0.809 in validation cohort. In the previous study [22], the authors combined the four imaging features related with CK19-positive HCCs to demonstrate a very high diagnostic specificity of 0.995 but also a low sensitivity of 0.211. Our final combined model demonstrated high diagnostic sensitivity and specificity in both cohorts.

Qualitative and quantitative analysis based on gadoxetic acid–enhanced MR imaging can be helpful for characterizing CK19-positive HCCs because the gene signatures of this subtype HCC are positively related to certain imaging traits [22, 23, 32]. Although a multi-sequence MRI protocol was available, only 11 and 6 radiomic features in arterial phase and HBP images were extracted for the best diagnostic perfor-

Table 3 Feature numbers after feature selection in different sequences

MR sequences	Intra-correlation coefficient	Inter-correlation coefficient	Reproducibility selection[a]	LASSO selection
T2-weighted image	0.192 ± 0.319	0.126 ± 0.215	305	0
Diffusion-weighted image	0.245 ± 0.317	0.132 ± 0.201	0	--
ADC maps image	0.532 ± 0.304	0.404 ± 0.261	0	--
Pre-contrast T1-weighted image	0.138 ± 0.296	0.066 ± 0.154	437	0
Arterial phase	0.180 ± 0.319	0.196 ± 0.305	175	11
Venous phase	0.156 ± 0.316	0.072 ± 0.163	328	4
Delayed phase	0.198 ± 0.316	0.117 ± 0.197	194	5
Hepatobiliary phase image	0.139 ± 0.294	0.083 ± 0.169	329	6

[a] Reproducibility selection with the inter- and intra- correlation coefficient (ICCs)

ADC, apparent diffusion coefficient

Table 4 Predictive efficacy of the clinical model, radiomics model and the combined model

Different models	AUC (95% CI)	Training dataset (n = 159)						Validation dataset (n = 68)						
		PNP	ACC	SENS	SPEC	PPV	NPV	AUC (95% CI)	PNP	ACC	SENS	SPEC	PPV	NPV
Clinical model	0.714 (0.624–0.803)	113	0.711	0.568	0.765	0.481	0.822	0.753 (0.636–0.871)	46	0.617	0.923	0.546	0.324	0.968
Radiomics model														
Arterial phase	0.847 (0.636–0.893)	117	0.736	0.841	0.696	0.514	0.920	0.764 (0.636–0.893)	49	0.726	0.692	0.727	0.375	0.909
Venous phase	0.912 (0.872–0.952)	132	0.830	0.977	0.774	0.623	0.989	0.636 (0.473–0.798)	44	0.647	0.385	0.709	0.238	0.830
Delay phase	0.847 (0.784–0.909)	123	0.774	0.773	0.774	0.567	0.899	0.683 (0.525–0.842)	39	0.574	0.692	0.545	0.265	0.882
Hepatobiliary phase	0.892 (0.847–0.937)	124	0.780	0.955	0.713	0.560	0.976	0.730 (0.578–0.882)	46	0.676	0.846	0.636	0.355	0.946
Arterial+ Hepatobiliary phase	0.951 (0.917–0.985)	134	0.843	0.955	0.800	0.646	0.979	0.822 (0.716–0.928)	48	0.706	0.846	0.673	0.379	0.949
Combined model	0.959 (0.929–0.989)	148	0.931	0.818	0.974	0.923	0.933	0.846 (0.730–0.963)	55	0.809	0.769	0.818	0.500	0.938

AUC, area under curve; *PNP*, predicted number of patients correctly classified; *ACC*, accuracy; *SENS*, sensitivity; *SPEC*, specificity; *NPV*, negative predictive value; *PPV*, positive predictive value

mance. DWI was excluded during feature selection for low reproducibility. DWI images have low spatial resolution and are subject to motion or magnetic artifacts, affecting the robustness of radiomics model construction. The radiomics signature included shape, intensity, and texture, which can reflect the complexity of the properties of the extracted tissue [33, 34]. For the fusion radiomics signature, two features in arterial phase and HBP corresponded to the biological characteristics of HCC with CK19-positive. "Ori_fos_minimum" is the minimum grey value of the intensity histogram, which reflects the signal intensity in the tumor. "Ori_Surface_to_volume_ratio" is the ratio of tumor surface to volume, a lower value of which indicates a more compact (sphere-like) shape. Hence, some morphological and radiological features of CK19-positive

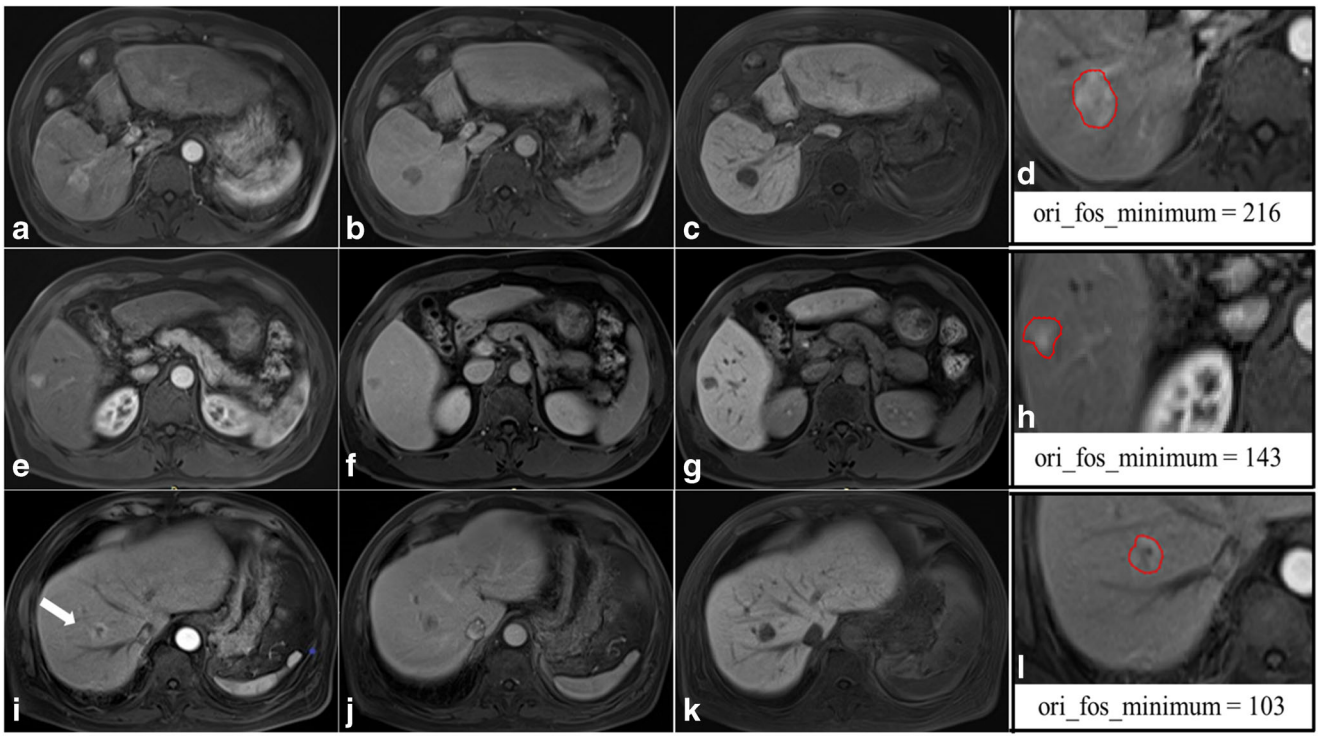

Fig. 2 Gadoxetic acid–enhanced MR imaging and comparisons of a significant radiomics feature between the three patients with single pathologically confirmed HCC. **a**–**d** the CK19-negative HCC showed typical enhancement pattern in a 68-year-old man. **a** Hyperintensity on arterial phase. **b** "Washout" on PVP. **c** Hypointensity on hepatobiliary phase (HBP). The radiomics signature of this patient was 0.137 and predicted as CK19 negative. **d** The radiomics feature extracted on arterial phase was "ori_fos_minimum" of 216. **e**–**h** The CK19-positive HCC also showed typical enhancement pattern in a 53-year-old man. **e** Hyperintensity on arterial phase. **f** "Washout" on PVP. **g** Hypointensity on HBP. The CK19 status was difficult to be characterized by imaging features. However, the radiomics signature of this patient was 0.678 and predicted as CK19 positive. **h** The radiomics feature "ori_fos_minimum" of 143. **i**–**l** the CK19-positive HCC in a 75-year-old man showed arterial rim enhancement (arrow) and radiomics features can further enhance the prediction probability of CK19 status (the radiomics signature was 0.974 and predicted as CK19 positive). **i** Rim enhancement on arterial phase. **j** "Washout" on PVP. **k** Hypointensity on HBP. **l** The radiomics feature "ori_fos_minimum" of 103

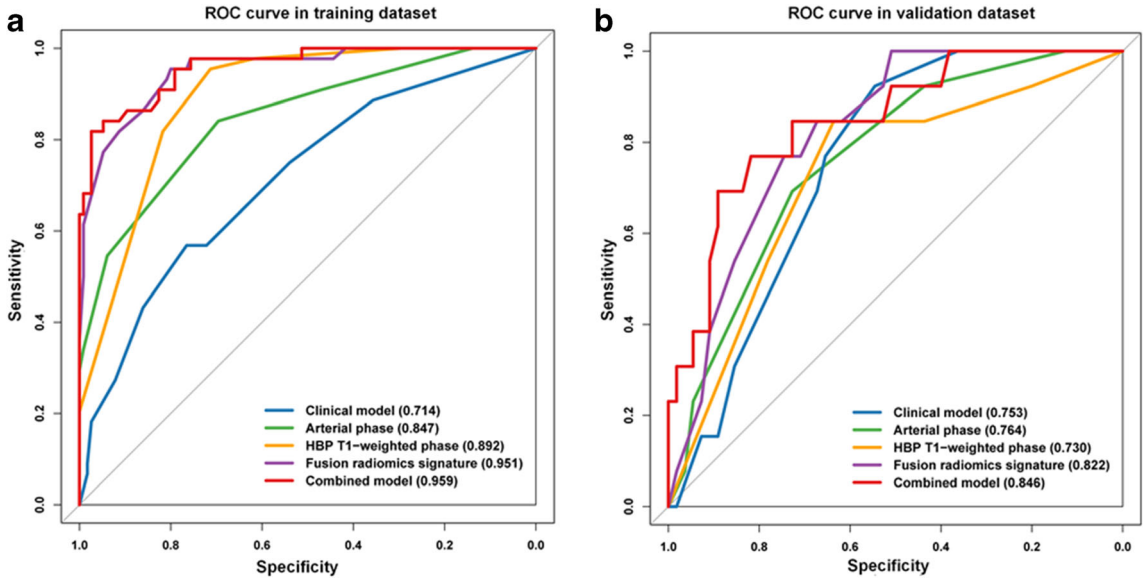

Fig. 3 Comparison of receiver operating characteristics (ROC) curves for predicting CK19 status of HCC. ROC curves of clinical factors, radiomics signatures in hepatobiliary phase and arterial phase images, the fusion radiomics signature, and the combined model that integrated with the clinical factors and the fusion radiomics signature in the (**a**) training and (**b**) validation dataset

HCC can be explained in a radiomics approach. Some previous studies also reported that higher tumor-to-liver signal intensity ratio on DWI and HBP images can quantitatively identify CK19-positive HCC [22, 35] while this method could be limited in reflecting the intratumoral heterogeneity and complexity of tumor morphology [35].

The clinicopathologic features of CK19-positive HCCs had no significant difference in training and validated cohorts. In line with previous studies [8, 9], serum AFP level could serve as a predictive marker for CK19 expression. As immunohistochemistry of HCC can be simultaneously positive for CK19 and AFP [10, 36], higher serum AFP level is a feature commonly associated with this subtype of HCCs. In clinical practice, serum AFP level can be easily obtained and incorporated into a nomogram for individualized risk estimation. For histology, CK19-positive HCCs were more likely to exhibit an

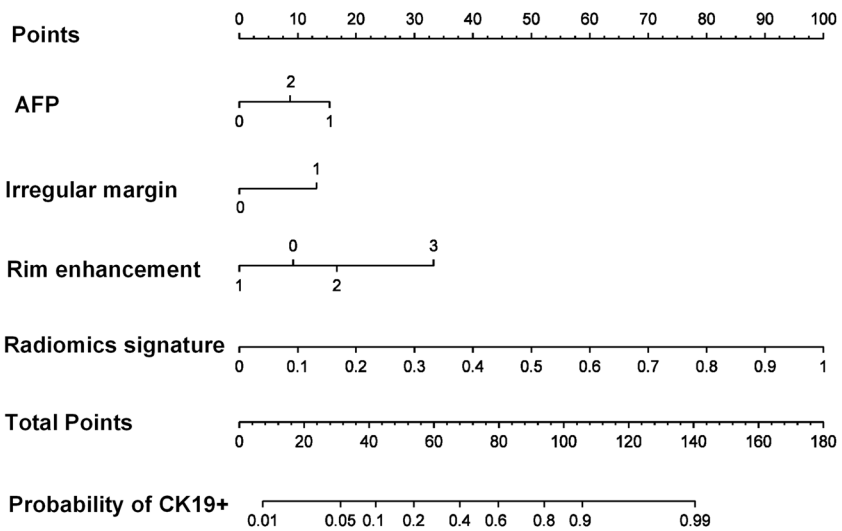

Fig. 4 Nomogram for predicting the positive of CK19 probabilities. The radiomics-based nomogram integrating the fusion radiomics signature extracted from hepatobiliary phase and arterial phase images, and clinical and morphologic risk factors including serum AFP level, irregular margin, and arterial rim enhancement pattern. For AFP, "0" refers to the level < 20 ng/mL, "1" refers to 20–400 ng/mL, and "2" refers to > 400 ng/mL. For irregular margin, "0" refers to absence of irregular margin, and "1" refers to presence of irregular margin. For arterial rim enhancement, "0" refers to absence of rim enhancement, and "1" refers to presence of arterial rim enhancement. "Radiomics signature" is the prediction probability of CK19 status of the combined model. "Total points" is the total score by adding all the single score obtained from AFP, irregular margin, arterial rim enhancement, and radiomics signature. The single score is obtained by draw a line straight up from the single feature axis to the point axis

aggressive phenotype, characterized by larger tumor size, poor differentiation, and presence of microvascular invasion [9, 37], although it was not statistically significant in our study.

Our results also showed that irregular tumor margin was associated with CK19 expression. CK19-positive HCCs were more likely to show perinodular extension, multinodular confluent, or infiltrative gross types [38]. Arterial rim enhancement pattern is frequently observed in intrahepatic cholangiocarcinomas or combined hepatocellular-cholangiocarcinoma. Jeong et al [23] reported that some CK19-positive HCCs showed persistent or progressive dynamic enhancement pattern, another characteristic imaging feature of intrahepatic cholangiocarcinoma. We hypothesized that during multistep hepatocarcinogenesis [39], CK19-positive HCCs may have an intermediate phenotype between biliary and mature hepatocyte differentiation, as CK19 is an important marker for hepatic progenitor cells. Interestingly, HCCs showing irregularly shaped rim-like enhancement have been especially reported to express higher CK19 levels with aggressive histopathologic features [40].

There were some limitations in our study. First, it is a retrospective study and may have selection bias. Second, the sample size of CK19-positive HCCs was relatively small. Third, CK19-positive was defined as a cutoff 5% of tumor cells to avoid false-positive results. The association between our predictive model and the graded degree of CK19 immunopositivity should be further assessed. Last, whether the predictive model can differentiate CK19-positive HCC from cholangiocarcinoma should be better validated as both tumors often demonstrate similar imaging features. However, the validation was limited by the inadequate sample of cholangiocarcinoma with gadoxetic acid–enhanced MR imaging in our institution.

In conclusion, the radiomics signatures derived from arterial phase and hepatobiliary phase images of gadoxetic acid–enhanced MR imaging can help predict CK19 status of HCC. A predictive nomogram incorporating radiomics signatures, preoperative serum AFP levels, irregular tumor margin, and arterial rim enhancement pattern demonstrated a significantly improved diagnostic performance in CK19 stratification of HCC.

Funding information This study has received funding by National Natural Science Foundation of China (No. 81227901, 81527805, 81571661); Chinese Academy of Sciences (No. GJJSTD20170004); the Shanghai Sailing Program (19YF1408100).

Compliance with ethical standards

Guarantor The scientific guarantor of this publication is Mengsu Zeng.

Conflict of interest The authors of this manuscript declare no relationships with any companies whose products or services may be related to the subject matter of the article.

Statistics and biometry No complex statistical methods were necessary for this paper.

Informed consent Written informed consent was obtained from all subjects (patients) in this study.

Written informed consent was waived by the Institutional Review Board.

Ethical approval Institutional Review Board approval was obtained.

Methodology
- Retrospective
- Diagnostic or prognostic study
- Performed at one institution

References

1. Ferlay J, Shin HR, Bray F, Forman D, Mathers C, Parkin DM (2010) Estimates of worldwide burden of cancer in 2008: GLOBOCAN 2008. Int J Cancer 127:2893–2917
2. Forner A, Reig M, Bruix J (2010) Hepatocellular carcinoma. Lancet 391:1301–1314
3. de Lope CR, Tremosini S, Forner A, Reig M, Bruix J (2012) Management of HCC. J Hepatol 56(Suppl 1):S75–S87
4. Forner A, Reig ME, de Lope CR, Bruix J (2010) Current strategy for staging and treatment: the BCLC update and future prospects. Semin Liver Dis 30:61–74
5. Mishra L, Banker T, Murray J et al (2009) Liver stem cells and hepatocellular carcinoma. Hepatology 49:318–329
6. Hoshida Y, Nijman SM, Kobayashi M et al (2009) Integrative transcriptome analysis reveals common molecular subclasses of human hepatocellular carcinoma. Cancer Res 69:7385–7392
7. Moll R, Franke WW, Schiller DL, Geiger B, Krepler R (1982) The catalog of human cytokeratins: patterns of expression in normal epithelia, tumors and cultured cells. Cell 31:11–24
8. Durnez A, Verslype C, Nevens F et al (2006) The clinicopathological and prognostic relevance of cytokeratin 7 and 19 expression in hepatocellular carcinoma. A possible progenitor cell origin. Histopathology 49:138–151
9. Kim H, Choi GH, Na DC et al (2011) Human hepatocellular carcinomas with "Stemness"-related marker expression: keratin 19 expression and a poor prognosis. Hepatology 54:1707–1717
10. Roncalli M, Park YN, Di Tommaso L (2010) Histopathological classification of hepatocellular carcinoma. Dig Liver Dis 42: S228–S234
11. Lee CW, Kuo WL, Yu MC et al (2013) The expression of cytokeratin 19 in lymph nodes was a poor prognostic factor for hepatocellular carcinoma after hepatic resection. World J Surg Oncol 11:136
12. Zhuang PY, Zhang JB, Zhu XD et al (2008) Two pathologic types of hepatocellular carcinoma with lymph node metastasis with distinct prognosis on the basis of CK19 expression in tumor. Cancer 112:2740–2748
13. Fatourou E, Koskinas J, Karandrea D et al (2015) Keratin 19 protein expression is an independent predictor of survival in human hepatocellular carcinoma. Eur J Gastroenterol Hepatol 27:1094–1102
14. Lee SH, Lee JS, Na GH, You YK, Kim DG (2017) Immunohistochemical markers for hepatocellular carcinoma prognosis after liver resection and liver transplantation. Clin Transplant 31
15. Kawai T, Yasuchika K, Ishii T et al (2015) Keratin 19, a cancer stem cell marker in human hepatocellular carcinoma. Clin Cancer Res 21:3081–3091

16. Katoh H, Ojima H, Kokubu A et al (2007) Genetically distinct and clinically relevant classification of hepatocellular carcinoma: putative therapeutic targets. Gastroenterology 133:1475–1486
17. Segal E, Sirlin CB, Ooi C et al (2007) Decoding global gene expression programs in liver cancer by noninvasive imaging. Nat Biotechnol 25:675–680
18. Rutman AM, Kuo MD (2009) Radiogenomics: creating a link between molecular diagnostics and diagnostic imaging. Eur J Radiol 70:232–241
19. Lambin P, Rios-Velazquez E, Leijenaar R et al (2012) Radiomics: extracting more information from medical images using advanced feature analysis. Eur J Cancer 48:441–446
20. Ma X, Wei J, Gu D et al (2019) Preoperative radiomics nomogram for microvascular invasion prediction in hepatocellular carcinoma using contrast-enhanced CT. Eur Radiol 29:3595–3605
21. Chen S, Feng S, Wei J et al (2019) Pretreatment prediction of immunoscore in hepatocellular cancer: a radiomics-based clinical model based on Gd-EOB-DTPA-enhanced MRI imaging. Eur Radiol 29:4177–4187
22. Choi SY, Kim SH, Park CK et al (2018) Imaging features of gadoxetic acid-enhanced and diffusion-weighted MR imaging for identifying cytokeratin 19-positive hepatocellular carcinoma: a retrospective observational study. Radiology 286:897–908
23. Jeong HT, Kim MJ, Kim YE, Park YN, Choi GH, Choi JS (2012) MRI features of hepatocellular carcinoma expressing progenitor cell markers. Liver Int 32:430–440
24. Hectors SJ, Wagner M, Bane O et al (2017) Quantification of hepatocellular carcinoma heterogeneity with multiparametric magnetic resonance imaging. Sci Rep 7:2452
25. Cong WM, Bu H, Chen J et al (2016) Practice guidelines for the pathological diagnosis of primary liver cancer: 2015 update. World J Gastroenterol 22:9279–9287
26. Gao Q, Qiu SJ, Fan J et al (2007) Intratumoral balance of regulatory and cytotoxic T cells is associated with prognosis of hepatocellular carcinoma after resection. J Clin Oncol 25:2586–2593
27. Yang XR, Xu Y, Shi GM et al (2008) Cytokeratin 10 and cytokeratin 19: predictive markers for poor prognosis in hepatocellular carcinoma patients after curative resection. Clin Cancer Res 14:3850–3859
28. Van Griethuysen JJM, Fedorov A, Parmar C et al (2017) Computational radiomics system to decode the radiographic phenotype. Cancer Res 77:e104–e107
29. Leijenaar RTH, Carvalho S, Velazquez ER et al (2013) Stability of FDG-PET radiomics features: an integrated analysis of test-retest and inter-observer variability. Acta Oncol 52:1391–1397
30. Tibshirani R (1997) The lasso method for variable selection in the Cox model. Stat Med 16:385–395
31. Kaminski B, Jakubczyk M, Szufel P (2018) A framework for sensitivity analysis of decision trees. Cent Eur J Oper Res 26:135–159
32. Taouli B, Hoshida Y, Kakite S et al (2017) Imaging-based surrogate markers of transcriptome subclasses and signatures in hepatocellular carcinoma: preliminary results. Eur Radiol 27:4472–4481
33. Boonzaier NR, Piccirillo SG, Watts C, Price SJ (2015) Assessing and monitoring intratumor heterogeneity in glioblastoma: how far has multimodal imaging come? CNS Oncol 4:399–410
34. Davnall F, Yip CS, Ljungqvist G et al (2012) Assessment of tumor heterogeneity: an emerging imaging tool for clinical practice? Insights Imaging 3:573–589
35. Kumar V, Gu Y, Basu S et al (2012) Radiomics: the process and the challenges. Magn Reson Imaging 30:1234–1248
36. Yamashita T, Forgues M, Wang W et al (2008) EpCAM and alpha-fetoprotein expression defines novel prognostic subtypes of hepatocellular carcinoma. Cancer Res 68:1451–1461
37. Kim H, Park YN (2014) Hepatocellular carcinomas expressing 'stemness'-related markers: clinicopathological characteristics. Dig Dis 32:778–785
38. Lee Y, Park H, Lee H et al (2018) The clinicopathological and prognostic significance of the gross classification of hepatocellular carcinoma. J Pathol Transl Med 52:85–92
39. Chiba T, Kamiya A, Yokosuka O, Iwama A (2009) Cancer stem cells in hepatocellular carcinoma: recent progress and perspective. Cancer Lett 286:145–153
40. Rhee H, An C, Kim H, Yoo JE, Park YN, Kim M (2018) Hepatocellular carcinoma with irregular rim-like arterial phase hyperenhancement: more aggressive pathologic features. Liver Cancer:1–17